All nanoparticle SnO_2/TiO_2 electron transporting layers processed at low temperature for efficient thin film perovskite solar cells

Guillermo Martínez-Denegri†, Silvia Colodrero†, Mariia Kramarenko†, Jordi Martorell*†‡*

† ICFO-Institut de Ciencies Fotoniques, The Barcelona Institute of Science and Technology, 08860 Castelldefels, Spain

‡ Departament de Física, Universitat Politecnica de Catalunya, Terrassa 08222, Spain

ABSTRACT

Solution processed metal halide perovskite materials have revealed outstanding optoelectronic features that make them uniquely suited for photovoltaic applications. Although a rapid progress has led to performances similar to inorganic thin film technologies, the fabrication method of some of the most widely used electron selective layers, based on either mesoporous architectures or high annealing temperatures, may limit yet a future large scale production. In that regard, planar perovskite solar cell configurations that can be processed at low temperatures are more desirable. Herein, we demonstrate that a few tens of nanometers thick bilayer, made of two types of inorganic oxide nanoparticles, can perform as a robust and low temperature processed electron selective contact for planar perovskite solar cells. Aside from boosting the average efficiency of planar opaque devices, the proposed method allowed us to preserve the main photovoltaic characteristics when thinner active layers, usually exhibiting a non-continuous morphology, were integrated for semi-transparent cells. By providing excellent electronic and coverage features against the bottom electrode, this novel configuration may hence offer an alternative route to approach future inexpensive printable methodologies for the fabrication of efficient low temperature perovskite solar cells.

KEYWORDS: nanoparticles, electron transporting layers, perovskite solar cells, low processing temperature, thin films.

INTRODUCTION

Robust, cost-effective and low temperature processed selective layers are necessary for a next generation of printable photovoltaics based on metal halide perovskite semiconductors. In a typical device configuration, the perovskite absorber is sandwiched in between an electron and a hole transporting layer (ETL and HTL), whose role is both to facilitate charge transport and to assist charge collection of photogenerated carriers towards their respective contact electrodes.[1–5] Despite the large variety of solution processed methods developed for the active layer engineering, the best performing devices, built under a n-i-p configuration, rely yet on TiO_2 ensembles that include compact and mesoporous films annealed at high temperature as the n-type material.[6–9] It may, however, constitute a major constraint not only for the manufacturing but also for the practical application of perovskite devices into flexible modules or monolithic tandem systems.

In an attempt to simplify the fabrication process, planar configurations without integrating the mesoporous TiO_2 layer have been pursued. But, in this case, the performance can be reduced due to a charge accumulation process caused by the poor charge extraction of TiO_2 and its smaller contact area with the perovskite layer.[10,11] Among the n-type inorganic materials reported until now, SnO_2 has demonstrated to be a promising alternative owing to its high electron mobility, wide band gap and long stability under UV illumination.[12–15] Many approaches including SnO_2 have been lately tested, ranging from thin compact layers[13,16] to combinations with mesoscopic structures[17,18] or doped-SnO_2.[19,20] However, either thin film deposition techniques that allow a precise control on both the thickness and the homogeneity of the ETL[21] or certain surface post-treatments[15,17,18,22] are still required to suppress undesired interfacial charge recombination pathways. In addition, some of the SnO_2 precursors[16,19,20,22–24] and post-treatment procedures[17,18] are often based on acidic solutions that may damage the transparent conductive oxide (TCO)

material employed as the bottom electrode of the cell. This imposes the use of chemically more resistant TCO substrates, such as fluorine tin oxide (FTO), while impeding their application on indium tin oxide (ITO) and other type of flexible conducting substrates. To combine high electron extraction and low interfacial recombination, a different path has considered the implementation of double inorganic ETLs displaying a more favorable energy level alignment between the bottom electrode and the perovskite materials,[25,26] although the use of either high temperature or acidic post-treatment procedures still limited their integration on a large variety of TCO substrates. An alternative route has also implemented passivating fullerene derivatives between the inorganic ETL and the perovskite layer to further improve the cell performance.[23,27,28]

In this paper, we fabricate a completely nanoparticulated bilayer, processed at low temperature by spin-coating technique, to perform as the electron selective contact in planar perovskite solar cells. The optimized double layer, made of SnO_2 and TiO_2 nanoparticles with a total thickness of a few tens of nanometers, is also compatible with the use of ITO substrates. We demonstrate first the excellent photovoltaic characteristics, reaching efficiencies above 15%, for planar $CH_3NH_3PbI_3$ perovskite devices with active layers of just 280 nm after the nanoparticle bilayer integration. On the other hand, the morphology of the nanoparticle bilayer showed to provide a suitable surface for the reliable fabrication of solar cells in which even thinner active layers presenting also non uniform coverage were employed. In fact, the relative increase in efficiency brought by the use of the double nanoparticle layer becomes more apparent as the thickness of the perovskite layer is further reduced as, for instance, in semi-transparent perovskite cells. In this latter case, the excellent FF values preserved for thinner absorber layers allowed us to obtain efficiencies up to 7% for a perovskite layer of just 90 nm in thickness, which corresponded to a 30% improvement when compared to a single TiO_2 ETL. These results suggest an effective

approach, fully processed at low temperature and compatible with the most common printable technologies, to afford realistic future applications of perovskite solar cells.

EXPERIMENTAL SECTION

Preparation of solution precursors

All commercially available chemicals were employed without any further purification. To get the TiO_2 nanoparticle precursor, 75 µL of TiO_2 nanoparticle suspension (Plasmachem, 20 wt% suspension in water, 4-8 nm) were mixed with 905 µL of methanol (Scharlau, 99.5%) and 20 µL of titanium diisopropoxidebis(acetylacetonate) ($Ti(acac)_2OiPr_2$, Sigma-Aldrich, 75 wt%). Based on previous reports,[29,30] the $Ti(acac)_2OiPr_2$ acts as a bridge between the surrounding nanoparticles, which thanks to a possible chelation of the acetylacetonate to the TiO_2 creates a coordinate ligand between them. A similar procedure was followed to obtain the SnO_2 nanoparticle precursor but, this time, 486.6 µL of SnO_2 nanoparticle suspension (Avantama AG, 2.5 wt% suspension in ethanol, 10 nm) were mixed with 500 µL of ethanol (Scharlau, 99.5%) and 13.4 µL of the organic titanate solution. Both suspensions were kept under stirring overnight before being used. Perovskite precursors were prepared inside a N_2 glovebox by dissolving methylammonium iodide (CH_3NH_3I, 1-Material, 99.5%) and lead (II) chloride ($PbCl_2$, Sigma-Aldrich, 98%) with a 3:1 molar ratio in dimethylformamide (Sigma-Aldrich, 99.8%) and using different weight concentrations depending on the desired film thickness (Supplementary Information, Figure S1). A 15 mg/ml poly[bis(4-phenyl)(2,4,6-trimethylphenyl)amine] (PTAA, Ossila) solution was prepared in toluene (Sigma-Aldrich, 99.8%) by keeping the mixture under stirring overnight at 60 °C. For the doping of the hole transporting material, 10 µL of a 170 mg/mL bis(trifluoromethylsulfonyl)amine lithium salt(Li-TFSI, Sigma-Aldrich, 99.95%) solution in

acetonitrile (Sigma-Aldrich, 99.8%) and 5 µL of 4-tert-butylpyridine (TBP, Sigma-Aldrich, 96%) were added to the solution.

Fabrication of perovskite solar cells

Two different types of ITO coated glass substrates were used depending on the final device configuration. For semi-transparent solar cells, two-stripe patterned ITO substrates (140 nm, 15 Ωsq^{-1}, Lumtec) were used, whereas for opaque ones full-covered ITO substrates (100 nm, 15 Ωsq^{-1}, Stuttgart) were employed. The electron transporting material, either as a single or as a double layer, was obtained by subsequently spin-coating the corresponding nanoparticle suspensions onto the cleaned ITO substrates at 6000 rpm, followed by a thermal annealing at 150 ºC during 30 minutes in air. The samples were then transferred into a glovebox for next fabrication steps. The perovskite solution was spin-coated on top of the electron transporting layer at 2500 rpm and the resulting films were annealed for 2 hours at 90 °C plus 20 minutes at 125 °C. After that, the PTAA solution was deposited at 2500 rpm on top of the perovskite layer. An 80 nm thick gold top contact layer was then evaporated in a high vacuum chamber (Lesker) for opaque cells. The deposition rate was adjusted to 0.6 Å /s and a metal mask was place to define an active area of 0.096 cm^2. For the semi-transparent devices, 12 nm of gold were deposited at a rate of 0.75 Å/s, followed by 40 nm of MoO_3 using an evaporation rate of 0.6 Å/s. This time a metal mask that conferred an active area of 0.06 cm^2 was used.

Thin film characterization

The optical transmission of the different samples was measured over the wavelength range of interest using a UV-vis-NIR spectrometer (Lambda 950, PerkinElmer). The surface morphology of the films was evaluated by atomic force microscopy operated in the tapping mode (AFM Dimension 3100, Veeco) and field emission scanning electron microscopy (FEG-SEM, FEI

Inspect F-EBL). The X-ray diffraction (XRD) patterns were recorded with a Bruker D8 Advance diffractometer (Bruker, Cu-Kα source). Film thickness values were determined employing a surface profilometer (Alpha-Step IQ Surface Profiler, KLA-Tencor).

Photovoltaic characterization

The photovoltaic performance of the fabricated solar cells was determined using an AM 1.5G solar simulator (Sun 3000, Abet Technologies). The illumination intensity corresponding to 100 $mWcm^{-2}$ was adjusted with a monocrystalline silicon reference cell (Hamamatsu) calibrated at the Fraunhofer Institute for Solar Energy Systems. The current voltage (J-V) curves were then recorded by scanning from positive to negative voltages (1.2 V to -0.2 V) using a Keithley 2400 SourceMeter and a scan speed of 350 mV/s. The statistical analysis of the solar cells performance was extracted from the results obtained in ten different devices. External quantum efficiency (EQE) analysis was performed using a quantum efficiency measurement system (QEX10, PV Measurements). In this case, the devices were illuminated using a monochromatic light coming from a xenon lamp. The spectral response of the calibrated silicon cell was used as a reference. All set of devices were tested under ambient conditions.

RESULTS

We started analyzing the morphology corresponding to the different ETL configurations studied, namely SnO_2 and TiO_2 monolayers and SnO_2/TiO_2 bilayers all made of nanoparticles, and its possible impact on the subsequent active layer growth. Atomic force microscopy (AFM) images corresponding to the different thin nanoparticulated layers, as well as top view scanning electron microscopy (SEM) images of perovskite films deposited on top, are presented in Figure 1. From the AFM images (Figure 1a-1c) it seems to be clear that, although SnO_2 and TiO_2 suspensions of about the same particle size were used, the former yielded a more uniform and compact film when

compared to the more porous texture like sponge of the latter. Interestingly, the structural characteristics of the perovskite layers (Figure 1d-1f) were also quite dissimilar in both cases. Whereas the formation of a polycrystalline material with clear individual grains could be inferred in the case of SnO_2, to differentiate the grain boundaries of the perovskite material with a TiO_2 underneath layer resulted less evident. Nonetheless, when we considered the SnO_2/TiO_2 bilayer, the perovskite morphology resembled in a remarkable way the same features exhibited by the single TiO_2 coating. These results suggest that the interface underlying the perovskite material may have a significant influence on its morphological characteristics. It is important to mention that exactly the same procedure for the perovskite deposition was carried out to avoid any undesired variation due to experimental conditions. Also, to ensure a good coverage of the perovskite layer at this time, a mixed halide perovskite solution with a high concentration (35 wt%) was prepared following the recipe reported by M. Lee et al.[31]

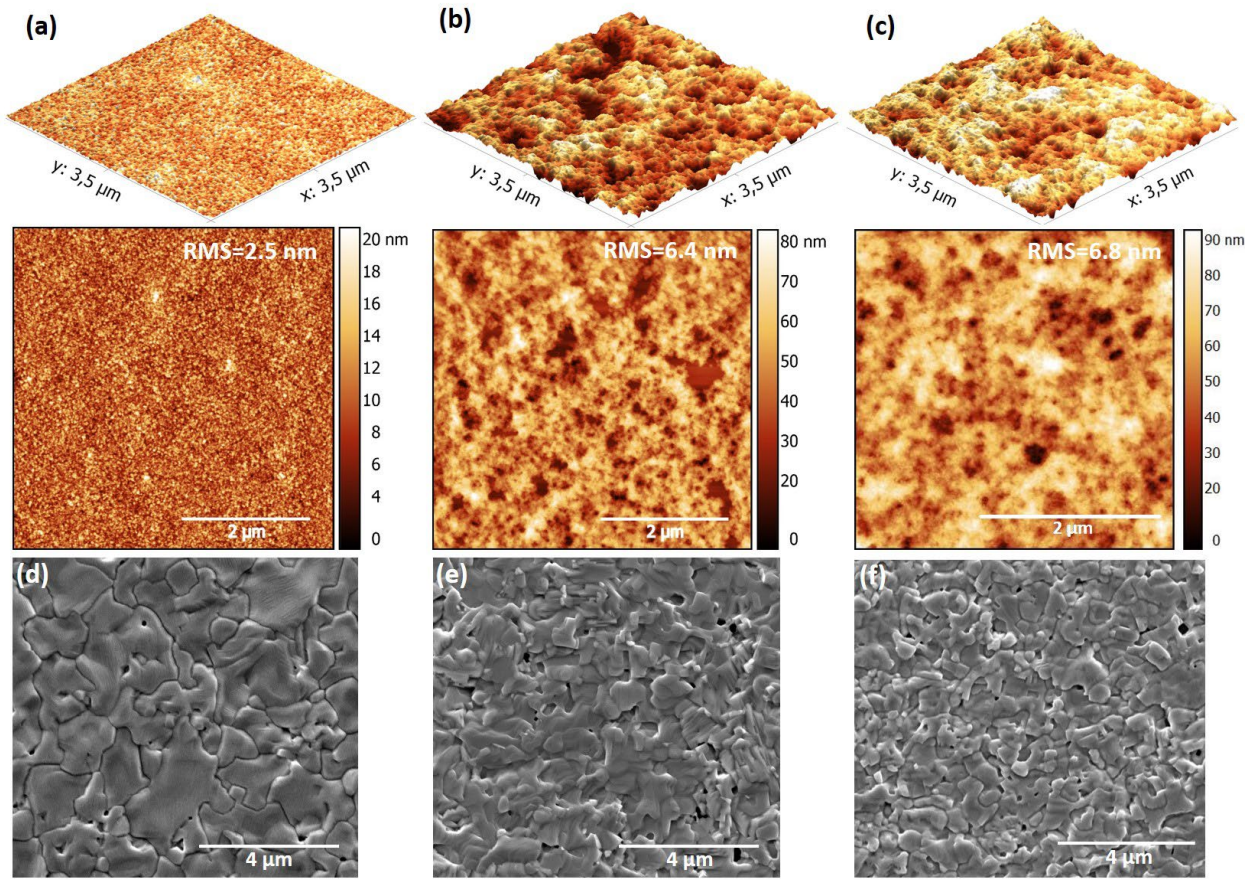

Figure 1. (a-c) AFM images corresponding to the SnO_2, TiO_2 and SnO_2/TiO_2 nanoparticle layers, respectively. The size of the SnO_2 and TiO_2 nanoparticles is 10 nm and 4-8 nm, respectively. (d-f) Top view SEM images displaying the different morphologies of perovskite layers when deposited on top of SnO_2, TiO_2 or SnO_2/TiO_2 nanoparticle layers, respectively.

Planar perovskite solar cells containing the different ETL combinations, either in monolayer or bilayer form, were then fabricated following the schematic diagram depicted in Figure 2a. Note that we considered only a SnO_2/TiO_2 bilayer due to the favorable energy band alignment between the corresponding conduction band of the inorganic oxides and the perovskite. In all cases, poly[bis(4-phenyl)(2,4,6-trimethylphenyl)amine] (PTAA) polymer was chosen as the p-type selective contact. The thicknesses measured for the fully spin coated n-i-p stack displaying the best

photovoltaic characteristics were 25 nm, 40 nm, 280 nm and 70 nm for the SnO_2, TiO_2, perovskite and PTAA layers, respectively. When the single ETL alternatives were considered, the optimal thickness found after experimental analysis corresponded to the values above indicated of 25 nm for SnO2 and 40 nm for TiO_2.

Figure 2b shows the typical current density-voltage (J-V) curves measured for perovskite solar cells integrating the different ETL combinations and displaying their photovoltaic parameters among the attained average values. As it can be appreciated, the double ETL exhibited slightly higher short circuit photocurrent (Jsc) and fill factor (FF) values when compared to the single TiO_2 layer, thus giving rise to the best photovoltaic behavior. On the contrary, the SnO_2 ETL based cells showed the lowest performance, mainly due to their poorer FF values. The photovoltaic parameters extracted from the different J-V curves, which are summarized also in Table 1 for comparison, yielded overall efficiencies of 14.9%, 14.2% and 8.6% for the SnO_2/TiO_2, TiO_2 and SnO_2 nanoparticle ETLs, respectively. The experimental details employed for the measurements can be found in the Experimental Section. The results obtained for the double ETL architecture might be explained as a consequence of the more effective charge transport and extraction processes, caused by the more suitable energy band matching and the higher electron mobility of SnO_2, as suggested elsewhere.[12,22,25] Besides, charge recombination taking place at the SnO_2/perovskite interface or at the grain boundaries of the absorbing material might be responsible for its lower performance, in good agreement with previous works.[32] Studying charge transport dynamics of the proposed device configuration to clarify the origin of the obtained results remains as one of the major challenges for future work.

The X ray diffraction (XRD) patterns of perovskite layers grown onto different types of substrates, mainly bare glass and SnO_2 or TiO_2 coated glass, can be also checked in Figure 2c.

Although almost the same diffraction pattern is observed for the whole set, the different peak intensity may evidence a preferred orientation in the case of the underlying nanoparticle TiO_2 layer when compared to the nanoparticle SnO_2 one. From the inset graph of Figure 2c, a slight shift of the diffraction peak is also detected for the perovskite grown onto SnO_2 nanoparticles, with a concomitant broadening of the peak that may be attributed, in principle, to the presence of smaller crystal size. These results support the conclusion that both the nature and the morphological features of the ETL play a crucial role on determining the characteristics of the perovskite material and, hence, the cell performance.

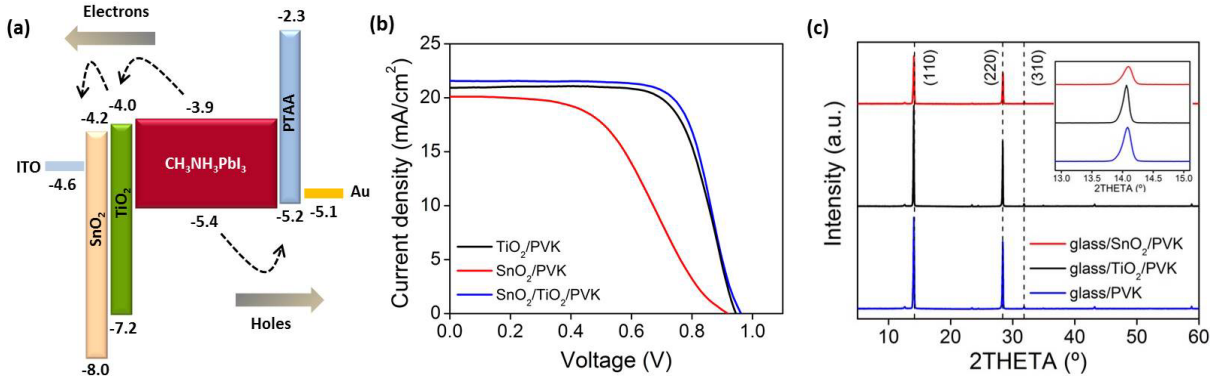

Figure 2. (a) Energy levels scheme for the different layers constituting the fabricated device. (b) J-V curves corresponding to perovskite solar cells displaying their photovoltaic parameters among the attained average values for the different ETL combinations: SnO_2 (red line), TiO_2 (black line) and SnO_2/TiO_2 (blue line). (c) XRD patterns of a 280 nm thick perovskite layer deposited on a bare glass substrate (blue), and onto TiO_2 (black) and SnO_2 nanoparticles (red).

Table 1. Photovoltaic parameters of the perovskite solar cells selected as representative of the average values integrating the single and double nanoparticle ETLs.

ETL configuration	Jsc (mA/cm^2)	Voc (V)	FF (%)	Efficiency (%)
TiO_2	20.9	0.95	71	14.2
SnO_2	20.1	0.93	46	8.6
SnO_2/TiO_2	21.7	0.97	71	14.9

To statistically analyze the results obtained for the set of fabricated devices, a box plot diagram of the photovoltaic parameter distribution is presented in Figure 3a-3d. In general, narrower dispersions in the parameters were obtained for the devices including TiO_2 and SnO_2/TiO_2 as the ETLs. For the latter case, we also identified both a slightly higher short circuit photocurrent (Jsc) and a significantly larger open circuit voltage (Voc) relative to the single ETL designs. In fact, the maximum values of Jsc and Voc reached for the double ETL architecture were about 0.3-0.7 mA/cm^2 and 40-50 mV higher than those obtained for the single ETLs. Also, the maximum efficiency was boosted to 15.2% for the SnO_2/TiO_2 ETL, whereas those were around 14.9% and 9.6% for the single TiO_2 and SnO_2 layers, respectively. Beyond these findings, these results suggest that completely nanoparticulated systems processed at low temperature may offer an easy and low cost route for the adequate ETL engineering in perovskite solar cells.

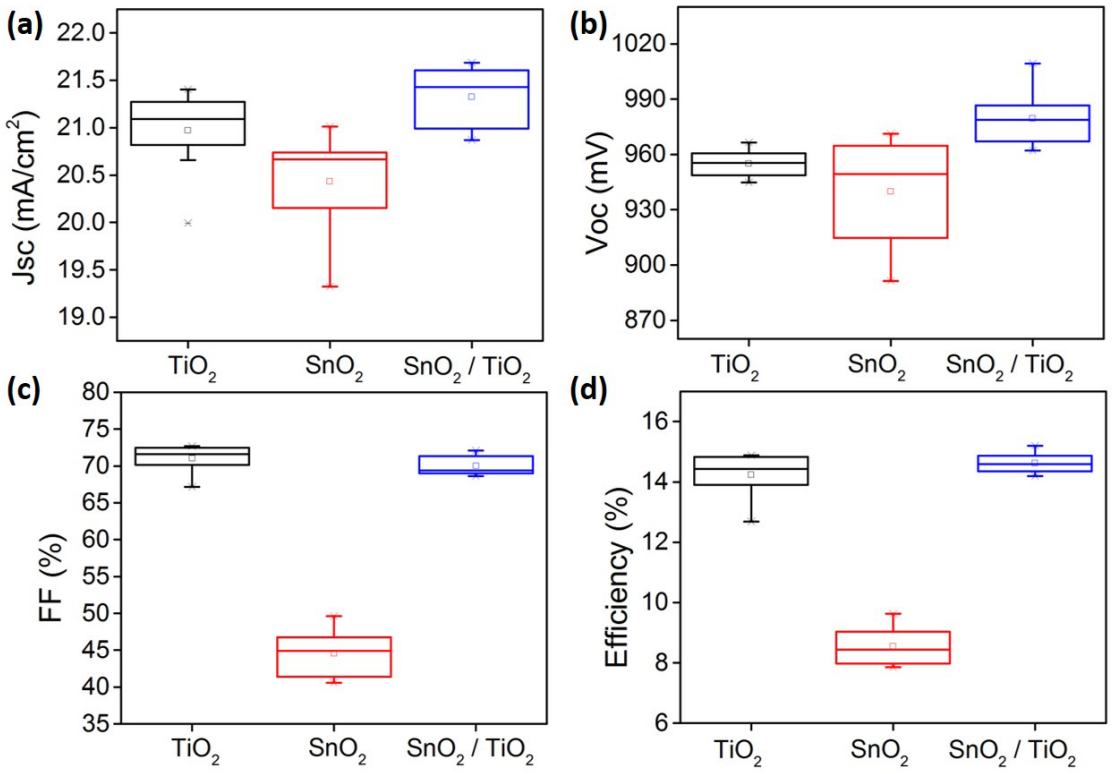

Figure 3. (a) Jsc, (b) Voc, (c) FF and (d) efficiency statistical analysis of perovskite solar cells fabricated using the different ETL combinations, mainly SnO_2 and TiO_2 monolayers and SnO_2/TiO_2 bilayer.

To evaluate the influence of the ITO coverage degree provided by the TiO_2 and the SnO_2/TiO_2 ETLs, due to the different compactness of the nanoparticle coatings, we also prepared a set of semi-transparent perovskite solar cells having the device configuration shown in Figure 4a. Non-continuous active layer morphology with a large absorber-free area is usually attained as the perovskite thickness is reduced. This aspect is fundamental to modify the transparency of the cell at will, but can also lead to shunting paths that will reduce its performance.[33–36] In our case, apart from varying the thickness of the perovskite absorber, an ultrathin Au contact covered by a protective MoO_3 layer were deposited by thermal evaporation as the top electrode. Although alternative semi-transparent top contact layers have been reported, ranging from silver

nanowires[37–39] and dielectric-metal-dielectric (DMD) architectures[40,41] to sputtered conductive oxides,[42–44] this combination ensures a reasonable good semitransparency over the visible without compromising the processing, performance and stability of the resulting devices.[45,46] The active layer thickness was then changed from 70 nm to 390 nm by modifying the concentration of the mixed halide perovskite solution while keeping the same deposition parameters. Even though special care during the crystallization process was taken, removal of excess material during the thermal annealing led to void spaces on the order of a few hundreds of nanometers for active layer thicknesses below 280 nm. Top view SEM images displayed in Figure 4c-4f show the morphology of such perovskite layers having thicknesses of 390 nm, 280 nm, 160 nm and 90 nm, respectively. A further analysis using an image processing program (ImageJ) allowed us to quantify both the coverage degree of the perovskite films and the average size of the open voids, as presented in Figure 4b.

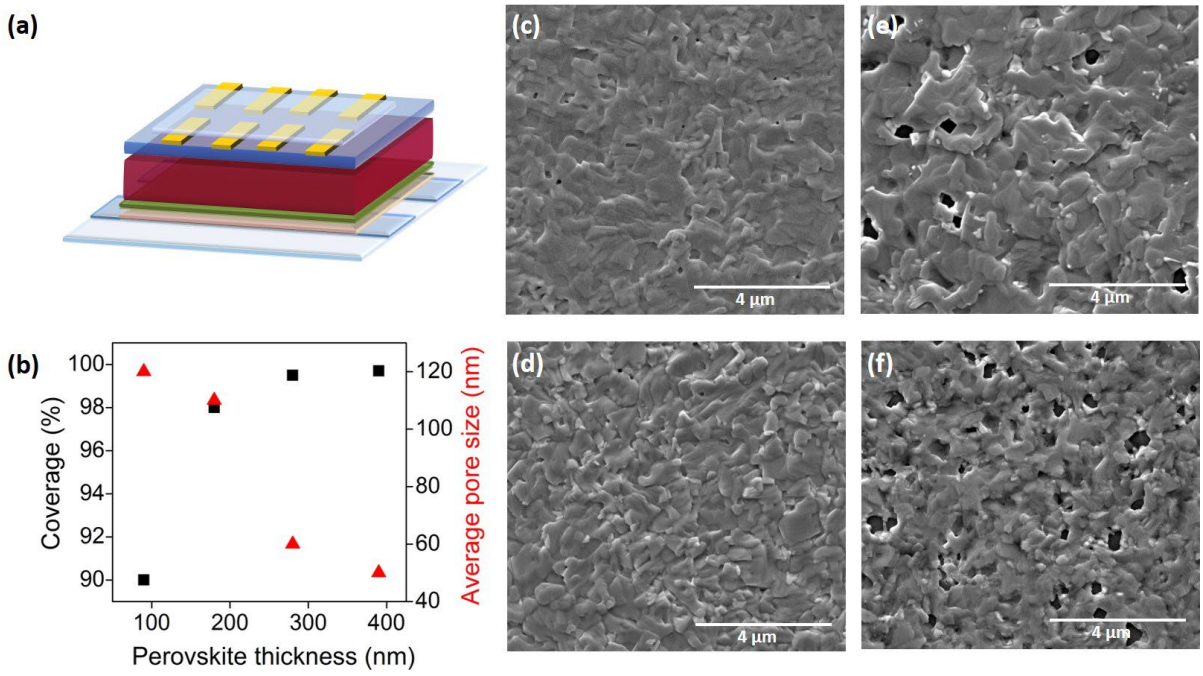

Figure 4. (a) Scheme of the proposed semi-transparent perovskite solar cell configuration. (b) Coverage degree (black) and average pore size (red) estimated for the deposited perovskite layers with different thicknesses. (c-f) Top view SEM images corresponding to perovskite layers of 390 nm, 280 nm, 160 nm and 90 nm in thickness, respectively.

Figure 5a-5b display the J-V and the external quantum efficiency (EQE) curves measured for the best performing semi-transparent devices based on the double layer architecture. For comparison, we also plotted in Figure 5a the data corresponding to solar cells based on a single TiO_2 ETL (dashed lines). We observed that, in both cases, the Jsc systematically increased with the active layer thickness as expected. However, those values were higher for the double ETL architecture and, this time, the increase in the Voc when compared to the single TiO_2 layer was superior as the perovskite thickness was reduced. This fact evidenced the good properties of SnO_2 nanoparticle coatings to effectively prevent shunting paths at the frontal ITO/perovskite interface, thus significantly suppressing charge recombination paths. Such conclusion is also supported by

the difficulty in fabricating devices only with the TiO_2 ETL and active layer thicknesses below 90 nm. Also, the remarkable FF values preserved for the thin absorber layers allowed us to obtain efficiencies up to 7% for a perovskite layer of 90 nm in thickness. On the other hand, cells fabricated using the highest concentration precursor led to lower FF and Voc values, which may be explained by a poorer control on the homogeneity of the films when a certain thickness is exceeded for this particular perovskite composition. To verify that the thickness of the nanoparticle TiO_2 layer was not limiting the cell performance, we also prepared devices with a TiO_2 thickness comparable to the double ETL one. The overall efficiency measured in devices with a perovskite layer of 90 nm, whose representative J-V curves are also plotted in Figure S2 of the Supplementary Information, show that a thicker TiO_2 single layer performs even worse than the standard (40 nm) TiO_2 alternative. These results support the fact that the superior performance of the double layer devices is not given by an increase on the thickness of the ETL.

From the EQE graph shown in Figure 5b, maximum values close to 90% were reached for the solar cells employing perovskite layers with thicknesses comprised between 390 nm and 160nm. However, both the reduced perovskite thickness and the presence of large void spaces affected predominantly the cell response over the longer wavelength range (500-800 nm), as can be yet appreciated for the 160 nm thick active layer. When even thinner films having a larger distribution of non-covered surface were employed, the maximum stood at around 60%, with an average at longer wavelengths of 30%. Figure 5c-5d display the transmittance spectra measured over the visible and the NIR range for the multilayered ITO/SnO_2/TiO_2/perovskite/PTAA configurations having the different active layer thicknesses and a picture of a complete semi-transparent cell made of a 70 nm thick perovskite layer, respectively.

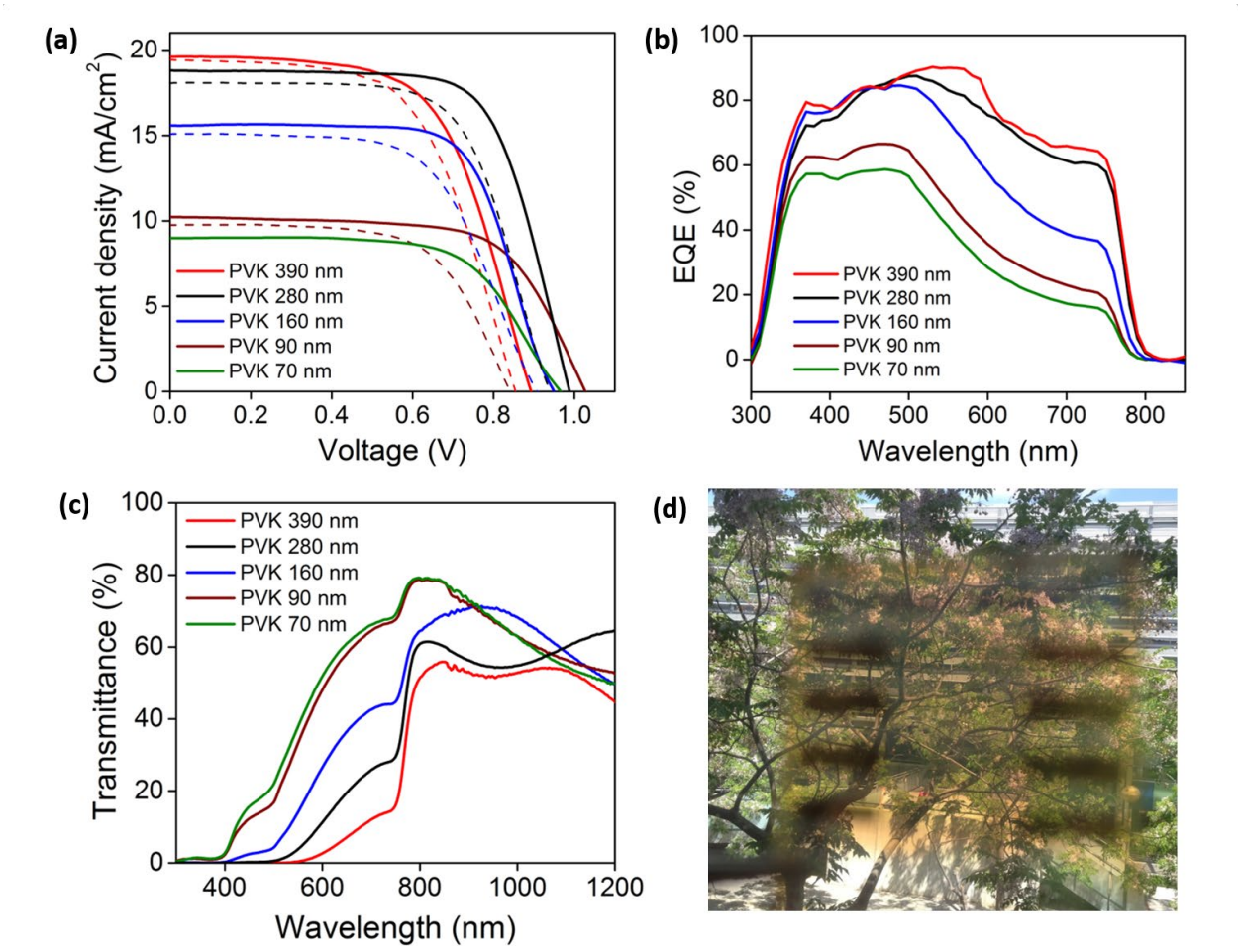

Figure 5. (a) J-V and (b) EQE curves corresponding to the best performing semi-transparent solar cells using different perovskite layer thicknesses. Data displayed as dashed and solid lines correspond to TiO_2 and SnO_2/TiO_2 based ETLs, respectively. Note that the same color code was applied to both graphs to identify each perovskite thickness. (c) Transmittance spectra acquired for the ITO/SnO_2/TiO_2/perovskite/PTAA stacks considering the different thicknesses of active layer. (d) Picture of a complete semi-transparent perovskite cell made of a 70 nm thick active layer.

Table 2 summarizes the photovoltaic parameters extracted from the J-V curves corresponding to the best performing devices, both opaque and semi-transparent. For the latter case, the resulting average transmittance (AVT) values were also included. This is particularly relevant for appealing applications in building integrated photovoltaic systems or silicon/perovskite tandem cells. Since

the effect of using the double layer architecture revealed no significant influence on the optical properties when compared to the single TiO_2 ETL, the same AVT value was obtained for both configurations (Figure S3, Supplementary Information). Since solar cells prepared with active layer thicknesses below 90 nm and containing only the TiO_2 ETL were not working properly, the corresponding parameters are not included in Table 2. More detailed information about the statistical distribution of the photovoltaic parameters obtained for the semi-transparent solar cells integrating the double ETL can be checked in Figure S4 of the Supporting Information.

The semi-transparent solar cells were also measured when illuminated from the thin metal contact side. The decrease in the Jsc in comparison to the results obtained when the devices are illuminated from the ITO is less than 24% for devices made of 280 nm thick perovskite layers. This decrease is similar or even lower than for other bifacial perovskite solar cells whose semi-transparent contact electrode is made of gold[41,47] or a different material.[48,49] Such performance show that devices fabricated with the configuration proposed in this paper have a potential application as bifacial solar cells, although further work may need to be carried out to further optimize the optoelectronic properties of the metal-dielectric contact. Those results can be also found in Figure S5 and Table S1 of the Supplementary Information.

Table 2. Photovoltaic parameters extracted from the analysis of the J-V curves for the complete set of best fabricated devices.

ETL configuration	Active Layer Thickness (nm)	Jsc (mA/cm^2)	Voc (V)	FF (%)	Efficiency (%)	AVT vis (%)*	AVT NIR (%)*
TiO_2	280	21.4	0.96	72.7	14.9	OPAQUE	OPAQUE
SnO_2	280	20.58	0.97	48.1	9.6		
SnO_2/TiO_2	280	21.7	0.98	71.3	15.2		
TiO_2	390	19.4	0.86	59.2	9.8	6 (5.2)	52.4 (35)
SnO_2/TiO_2	390	19.6	0.90	61.2	10.7		
TiO_2	280	18.1	0.94	65.8	11.2	12.6 (8.2)	62 (40.5)
SnO_2/TiO_2	280	18.8	0.99	69.5	12.9		
TiO_2	160	15	0.91	65.3	8.9	22.6 (12.3)	65 (40)
SnO_2/TiO_2	160	15.6	0.98	67.7	10.3		
TiO_2	90	9.7	0.85	65.5	5.4	40 (20)	64.5 (36)
SnO_2/TiO_2	90	10.2	1.03	66	6.9		
SnO_2/TiO_2	70	9	0.97	64.4	5.6	42.1 (27)	64 (39.3)

*Values in parentheses correspond to the AVT data obtained for complete devices including the top electrode.

DISCUSSION

A variety of strategies have been developed in the past years within the context of semi-transparent perovskite solar cells. In order to allow a more practical comparison of the results presented along this manuscript with previous works, we summarized in Table 3 some of the most outstanding results reported in the literature up to now. To do so, we chose semi-transparent solar cells using thin (<300 nm) perovskite films, fabricated through low temperature processes and with a planar configuration, so they are comparable to the present study. In terms of the

photovoltaic parameters our devices resemble the performance of previous works, being the Jsc in most of the cases superior to those presented in Table 3. However, most of the works included on it are based on device configurations that employ the same buffer layers as HTL and ETL (PEDOT:PSS and PCBM, respectively) and that focus their analysis on the optimization of the semi-transparent contact electrode and/or the perovskite fabrication method. On the other hand, only the work reported by Tiwari et al.[48] uses a n-i-p configuration for the fabrication of the low temperature planar semi-transparent solar cells. It is important to remark that, in our case, we deal with the optimization of the semi-transparent devices paying attention to low temperature alternatives by including the use of nanoparticles. The most critical point here is that of achieving a good layer interface and coverage as to provide efficient devices even with very thin perovskite films, which usually exhibit a non-continuous morphology. As we have demonstrated, the use of the optimized nanoparticle bilayers, processed at low temperature and with thickness values of a few tens of nanometers, gives rise to enhanced photovoltaic parameters of the solar cell. Although further insight into the origin of such improvements might be obtained from charge dynamic studies, the experimental results obtained suggest that electron-hole recombination is effectively decreased with the double ETL architecture. To the best of our knowledge, there are no similar works in which extremely thin (<100 nm) perovskite solar cells are fabricated using a n-i-p configuration and fulfilling the low temperature and planar perovskite conditions. Table S2 of the Supplementary Information shows a summary of the solar cell performances of opaque devices having the same characteristics than those in Table 3. Here again, higher Jsc and PCE values are mostly obtained with the double ETL architecture proposed in this paper when considering equivalent active layer thicknesses.

Table 3. Summary of the semi-transparent solar cell photovoltaic parameters extracted from the literature for approaches based on low temperature processes and planar device configurations.

Work	Configuration	Active Layer Thickness (nm)	Jsc (mA/cm^2)	Voc (V)	FF (%)	Efficiency (%)
Ref. [48][48]	FTO/ZnO/PCBM/$MAPbI_3$ /Spiro/MoO_3/ In_2O_3:H	280	17.4	1.1	73.6	14.1
Ref. [49][49]	ITO/PEDOT:PSS/$MAPbI_3$ /PCBM/BCP/Ag/MoO_3	270	17.73	1.05	72.5	13.49
		160	14.67	0.95	62.9	8.8
Ref. [39][39]	ITO/PEDOT:PSS/$MAPbI_3$ /PCBM/Ag NWs	100	14.9	0.98	72.1	10.2
		70	11.22	0.97	70.5	7.9
Ref. [37][37]	ITO/PEDOT:PSS/$MAPbI_3$ /PCBM/AZO/ ITO	275	16.5	0.95	77	12.3
Ref. [50][50]	ITO/PEDOT:PSS/$MAPbI_3$ /PCBM/ZnO/AgNWs/ Dielectric Mirror	40	6.33	1.03	65.6	4.3
Ref. [51][51]	ITO/PEDOT:PSS/$MAPbI_3$ /PCBM/Ag NWs	270	18.17	1.04	75	14.17
		150	15.00	1.00	71	10.55
		80	12.67	0.96	60	7.3
Ref. [52][52]	ITO/PEDOT:PSS/$MAPbI_3$ /PCBM/BCP/ IZO	260	17.2	1.05	70	12.8
Ref. [53][53]	ITO/PEDOT:PSS/$MAPbI_3$ /PCBM/AZO/SnO_x/Ag/ SnO_x	190	17.6	0.87	77.5	11.8
Ref. [54][54]	ITO/PEDOT:PSS/$MAPbI_3$ /ZnO/Ag Nws/PET/Al_2O_3	220	15.87	0.96	69.7	10.55

CONCLUSIONS

In conclusion, we have demonstrated that an all nanoparticle bilayer system, deposited by spin-coating and processed at low temperature, can perform as an effective electron selective layer for thin perovskite solar cells. By adequately selecting the inorganic oxide materials to provide a suitable energy band alignment with the perovskite, we confirmed an increase in the efficiency of opaque devices from 14.9% to 15.2%. The proposed bilayer was composed of SnO_2 and TiO_2 nanoparticles, having thicknesses of 25 nm and 40 nm, respectively. In addition, when we considered thinner absorber layers with a lower degree of coverage for semi-transparent photovoltaic applications, the enhancement effect observed by using the SnO_2/TiO_2 bilayer was significantly more pronounced. A feasible explanation for it could be found in the excellent properties of SnO_2 coatings to effectively prevent shunting paths in the cell, which allowed us to preserve remarkable FF values for devices constructed with active layers below 100 nm in thickness. Up to 30% improvement in the final performance could be obtained by employing the proposed strategy in such kind of semi-transparent cells, which is particularly attractive for applications that require specific aesthetic or transparency features due to its easy and low cost processing.

ASSOCIATED CONTENT

Supporting Information.

The supporting information is available free of charge on the ACS Publications website.

Precursor concentration-perovskite layer thickness plot, J-V curves comparison for different ETL thickness and composition, transmittance spectra of TiO_2 and SnO_2/TiO_2 based solar cells, box plot diagram of the different photovoltaic parameters for the different semi-transparent solar cells

containing the SnO_2/TiO_2 bilayer and photovoltaic results for the devices illuminated from the thin metal contact electrode. (PDF)

AUTHOR INFORMATION

Corresponding Authors

*E-mail: silvia.colodrero@icfo.eu

*E-mail: jordi.martorell@icfo.eu

Author Contributions

G. Martínez-Denegri and S.Colodrero designed the experiments and carried out the fabrication and characterization, both optical and photovoltaic, of the devices. G. Martínez-Denegri and M. Kramarenko conducted the SEM and AFM characterization of perovskite films. S.Colodrero and G. Martínez-Denegri wrote the manuscript with the assistance of all other authors. J. Martorell conceived the project and coordinated all the work.

Notes

The authors declare no competing financial interest.

ACKNOWLEDGMENT

This work was supported by the financial support from the Spanish MINECO (Severo Ochoa program, grant No.: SEV-2015-0522), the MINECO and the Fondo Europeo de Desarrollo Regional FEDER (grant No.: MAT2014-52985-R), the Fundació Privada Cellex, the CERCA programme from the Generalitat de Catalunya, and from the EC FP7 Program (ICT-2011.35) under grant agreement n° NMP3-SL-2013-604506.

REFERENCES

(1) Juarez-Perez, E. J.; Wussler, M.; Fabregat-Santiago, F.; Lakus-Wollny, K.; Mankel, E.; Mayer, T.; Jaegermann, W.; Mora-Sero, I. Role of the Selective Contacts in the Performance of Lead Halide Perovskite Solar Cells. *J. Phys. Chem. Lett.* **2014**, *5*, 680–685.

(2) Marchioro, A.; Teuscher, J.; Friedrich, D.; Kunst, M.; van de Krol, R.; Moehl, T.; Grätzel, M.; Moser, J.-E. Unravelling the Mechanism of Photoinduced Charge Transfer Processes in Lead Iodide Perovskite Solar Cells. *Nat. Photonics* **2014**, *8*, 250–255.

(3) Seo, J.; Noh, J. H.; Seok, S. Il. Rational Strategies for Efficient Perovskite Solar Cells. *Acc. Chem. Res.* **2016**, *49*, 562–572.

(4) Yang, G.; Tao, H.; Qin, P.; Ke, W.; Fang, G. Recent Progress in Electron Transport Layers for Efficient Perovskite Solar Cells. *J. Mater. Chem. A* **2016**, *4*, 3970–3990.

(5) Mahmood, K.; Sarwar, S.; Mehran, M. T. Current Status of Electron Transport Layers in Perovskite Solar Cells: Materials and Properties. *RSC Adv.* **2017**, *7*, 17044–17062.

(6) Saliba, M.; Matsui, T.; Domanski, K.; Seo, J.-Y.; Ummadisingu, A.; Zakeeruddin, S. M.; Correa-Baena, J.-P.; Tress, W. R.; Abate, A.; Hagfeldt, A.; Gratzel, M. Incorporation of Rubidium Cations into Perovskite Solar Cells Improves Photovoltaic Performance. *Science* **2016**, *354*, 206–209.

(7) Bi, D.; Yi, C.; Luo, J.; Décoppet, J.-D.; Zhang, F.; Zakeeruddin, S. M.; Li, X.; Hagfeldt, A.; Grätzel, M. Polymer-Templated Nucleation and Crystal Growth of Perovskite Films for Solar Cells with Efficiency Greater than 21%. *Nat. Energy* **2016**, *1*, 16142.

(8) Yang, W. S.; Park, B.-W.; Jung, E. H.; Jeon, N. J.; Kim, Y. C.; Lee, D. U.; Shin, S. S.; Seo,

J.; Kim, E. K.; Noh, J. H.; Seok, S. Il. Iodide Management in Formamidinium-Lead-Halide–based Perovskite Layers for Efficient Solar Cells. *Science* **2017**, *356*, 1376–1379.

(9) Yang, W. S.; Noh, J. H.; Jeon, N. J.; Kim, Y. C.; Ryu, S.; Seo, J.; Seok, S. Il. High-Performance Photovoltaic Perovskite Layers Fabricated through Intramolecular Exchange. *Science* **2015**, *348*, 1234–1237.

(10) Pascoe, A. R.; Yang, M.; Kopidakis, N.; Zhu, K.; Reese, M. O.; Rumbles, G.; Fekete, M.; Duffy, N. W.; Cheng, Y. B. Planar versus Mesoscopic Perovskite Microstructures: The Influence of CH3NH3PbI3 Morphology on Charge Transport and Recombination Dynamics. *Nano Energy* **2016**, *22*, 439–452.

(11) Huang, F.; Pascoe, A. R.; Wu, W. Q.; Ku, Z.; Peng, Y.; Zhong, J.; Caruso, R. A.; Cheng, Y. B. Effect of the Microstructure of the Functional Layers on the Efficiency of Perovskite Solar Cells. *Adv. Mater.* **2017**, *29*, 1601715.

(12) Tiwana, P.; Docampo, P.; Johnston, M. B.; Snaith, H. J.; Herz, L. M. Electron Mobility and Injection Dynamics in Mesoporous ZnO, SnO2, and TiO2 Films Used in Dye-Sensitized Solar Cells. *ACS Nano* **2011**, *5*, 5158–5166.

(13) Anaraki, E. H.; Kermanpur, A.; Steier, L.; Domanski, K.; Matsui, T.; Tress, W.; Saliba, M.; Abate, A.; Grätzel, M.; Hagfeldt, A.; Correa-Baena, J. P. Highly Efficient and Stable Planar Perovskite Solar Cells by Solution-Processed Tin Oxide. *Energy Environ. Sci.* **2016**, *9*, 3128–3134.

(14) Snaith, H. J.; Ducati, C. SnO2-Based Dye-Sensitized Hybrid Solar Cells Exhibiting near Unity Absorbed Photon-to-Electron Conversion Efficiency. *Nano Lett.* **2010**, *10*, 1259–

1265.

(15) Rao, H. S.; Chen, B. X.; Li, W. G.; Xu, Y. F.; Chen, H. Y.; Kuang, D. Bin; Su, C. Y. Improving the Extraction of Photogenerated Electrons with SnO2 Nanocolloids for Efficient Planar Perovskite Solar Cells. *Adv. Funct. Mater.* **2015**, *25*, 7200–7207.

(16) Ke, W.; Fang, G.; Liu, Q.; Xiong, L.; Qin, P.; Tao, H.; Wang, J.; Lei, H.; Li, B.; Wan, J.; Yang, G.; Yan, Y. Low-Temperature Solution-Processed Tin Oxide as an Alternative Electron Transporting Layer for Efficient Perovskite Solar Cells. *J. Am. Chem. Soc.* **2015**, *137*, 6730–6733.

(17) Li, Y.; Zhu, J.; Huang, Y.; Liu, F.; Lv, M.; Chen, S.; Hu, L.; Tang, J.; Yao, J.; Dai, S. Mesoporous SnO_2 Nanoparticle Films as Electron-Transporting Material in Perovskite Solar Cells. *RSC Adv.* **2015**, *5*, 28424–28429.

(18) Zhu, Z.; Zheng, X.; Bai, Y.; Zhang, T.; Wang, Z.; Xiao, S.; Yang, S. Mesoporous SnO2 Single Crystals as an Effective Electron Collector for Perovskite Solar Cells. *Phys. Chem. Chem. Phys.* **2015**, *17*, 18265–18268.

(19) Bai, Y.; Fang, Y.; Deng, Y.; Wang, Q.; Zhao, J.; Zheng, X.; Zhang, Y.; Huang, J. Low Temperature Solution-Processed Sb:SnO2 Nanocrystals for Efficient Planar Perovskite Solar Cells. *ChemSusChem* **2016**, *9*, 2686–2691.

(20) Ren, X.; Yang, D.; Yang, Z.; Feng, J.; Zhu, X.; Niu, J.; Liu, Y.; Zhao, W.; Liu, S. F. Solution-Processed Nb:SnO_2 Electron Transport Layer for Efficient Planar Perovskite Solar Cells. *ACS Appl. Mater. Interfaces* **2017**, *9*, 2421–2429.

(21) Correa Baena, J. P.; Steier, L.; Tress, W.; Saliba, M.; Neutzner, S.; Matsui, T.; Giordano,

F.; Jacobsson, T. J.; Srimath Kandada, A. R.; Zakeeruddin, S. M.; Petrozza, A.; Abate, A.; Nazeeruddin, M. K; Grätzel, M.; Hagfeldt, A. Highly Efficient Planar Perovskite Solar Cells through Band Alignment Engineering. *Energy Environ. Sci.* **2015**, *8*, 2928–2934.

(22) Huang, X.; Hu, Z.; Xu, J.; Wang, P.; Wang, L.; Zhang, J.; Zhu, Y. Low-Temperature Processed SnO2 Compact Layer by Incorporating TiO2 Layer toward Efficient Planar Heterojunction Perovskite Solar Cells. *Sol. Energy Mater. Sol. Cells* **2017**, *164*, 87–92.

(23) Kegelmann, L.; Wolff, C. M.; Omondi, C. A.; Lang, F.; Unger, E. L.; Korte, L.; Dittrich, T.; Neher, D.; Rech, B.; Albrecht, S. It Takes Two to Tango – Double-Layer Selective Contacts in Perovskite Solar Cells for Improved Device Performance and Reduced Hysteresis. *ACS Appl. Mater. Interfaces* **2017**, *9*, 17245–17255.

(24) Ke, W.; Zhao, D.; Xiao, C.; Wang, C.; Cimaroli, A. J.; Grice, C. R.; Yang, M.; Li, Z.; Jiang, C.-S.; Al-Jassim, M.; Zhu, K; Kanatzidis, M. G.; Fang, G.; Yan, Y. Cooperative Tin Oxide Fullerene Electron Selective Layers for High-Performance Planar Perovskite Solar Cells. *J. Mater. Chem. A* **2016**, *4*, 14276–14283.

(25) Xu, X.; Zhang, H.; Shi, J.; Dong, J.; Luo, Y.; Li, D.; Meng, Q. Highly Efficient Planar Perovskite Solar Cells with a TiO_2 /ZnO Electron Transport Bilayer. *J. Mater. Chem. A* **2015**, *3*, 19288–19293.

(26) Okamoto, Y.; Suzuki, Y. Mesoporous BaTiO3/TiO2 Double Layer for Electron Transport in Perovskite Solar Cells. *J. Phys. Chem. C* **2016**, *120*, 13995–14000.

(27) Li, Y.; Zhao, Y.; Chen, Q.; Yang, Y.; Liu, Y.; Hong, Z.; Liu, Z.; Hsieh, Y. T.; Meng, L.; Li, Y.; Yang, Y;. Multifunctional Fullerene Derivative for Interface Engineering in Perovskite

Solar Cells. *J. Am. Chem. Soc.* **2015**, *137*, 15540–15547.

(28) Cui, C.; Li, Y.; Li, Y. Fullerene Derivatives for the Applications as Acceptor and Cathode Buffer Layer Materials for Organic and Perovskite Solar Cells. *Adv. Energy Mater.* **2017**, *7*, 1601251.

(29) Chen, H. J.; Wang, L.; Chiu, W. Y. Chelation and Solvent Effect on the Preparation of Titania Colloids. *Mater. Chem. Phys.* **2007**, *101*, 12–19.

(30) Wojciechowski, K.; Saliba, M.; Leijtens, T.; Abate, A.; Snaith, H. J. Sub-150 ºC Processed Meso-Superstructured Perovskite Solar Cells with Enhanced Efficiency. *Energy Environ. Sci.* **2014**, *7*, 1142–1147.

(31) Lee, M. M.; Teuscher, J.; Miyasaka, T.; Murakami, T. N.; Snaith, H. J. Efficient Hybrid Solar Cells Based on Meso-Superstructured Organometal Halide Perovskites. *Science* **2012**, *338*, 643–647.

(32) Nie, W.; Tsai, H.; Asadpour, R.; Blancon, J.-C.; Neukirch, A. J.; Gupta, G.; Crochet, J. J.; Chhowalla, M.; Tretiak, S.; Alam, M. A.; Wang, H. L.; Mohite, A. D. High-Efficiency Solution-Processed Perovskite Solar Cells with Millimeter-Scale Grains. *Science* **2015**, *347*, 522–525.

(33) Aharon, S.; Layani, M.; Cohen, B.-E.; Shukrun, E.; Magdassi, S.; Etgar, L. Self-Assembly of Perovskite for Fabrication of Semi-Transparent Perovskite Solar Cells. *Adv. Mater. Interfaces* **2015**, 2, 1500118.

(34) Hörantner, M. T.; Nayak, P. K.; Mukhopadhyay, S.; Wojciechowski, K.; Beck, C.; McMeekin, D.; Kamino, B.; Eperon, G. E.; Snaith, H. J. Shunt-Blocking Layers for

Semitransparent Perovskite Solar Cells. *Adv. Mater. Interfaces* **2016**, *3*, 1500837.

(35) Eperon, G. E.; Burlakov, V. M.; Goriely, A.; Snaith, H. J. Neutral Color Semitransparent Microstructured Perovskite Solar Cells. *ACS Nano* **2014**, *8*, 591–598.

(36) You, P.; Liu, Z.; Tai, Q.; Liu, S.; Yan, F. Efficient Semitransparent Perovskite Solar Cells with Graphene Electrodes. *Adv. Mater.* **2015**, *27*, 3632–3638.

(37) Bailie, C. D.; Christoforo, M. G.; Mailoa, J. P.; Bowring, A. R.; Unger, E. L.; Nguyen, W. H.; Burschka, J.; Pellet, N.; Lee, J. Z.; Grätzel, M.; Noufi, R.; Buonassisi, T.; Salleo, A.; McGehee, M. D. Semi-Transparent Perovskite Solar Cells for Tandems with Silicon and CIGS. *Energy Environ. Sci.* **2015**, *8*, 956–963.

(38) Guo, F.; Azimi, H.; Hou, Y.; Przybilla, T.; Hu, M.; Bronnbauer, C.; Langner, S.; Spiecker, E.; Forberich, K.; Brabec, C. J. High-Performance Semitransparent Perovskite Solar Cells with Solution-Processed Silver Nanowires as Top Electrodes. *Nanoscale* **2015**, *7*, 1642–1649.

(39) Quiroz, C. O. R.; Levchuk, L.; Bronnbauer, C.; Salvador, M.; Forberich, K.; Heumueller, T.; Hou, Y.; Schweizer, P.; Spiecker, E.; Brabec, C. J. Pushing Efficiency Limits for Semitransparent Perovskite Solar Cells. *J. Mater. Chem. A* **2015**, *3*, 24071–24081.

(40) Yang, Y. (Michael); Chen, Q.; Hsieh, Y.-T.; Song, T.-B.; Marco, N. De; Zhou, H.; Yang, Y. Multilayer Transparent Top Electrode for Solution Processed Perovskite/Cu(In,Ga)(Se,S) $_2$ Four Terminal Tandem Solar Cells. *ACS Nano* **2015**, *9*, 7714–7721.

(41) Della Gaspera, E.; Peng, Y.; Hou, Q.; Spiccia, L.; Bach, U.; Jasieniak, J. J.; Cheng, Y. B.

Ultra-Thin High Efficiency Semitransparent Perovskite Solar Cells. *Nano Energy* **2015**, *13*, 249–257.

(42) Duong, T.; Lal, N.; Grant, D.; Jacobs, D.; Zheng, P.; Rahman, S.; Shen, H.; Stocks, M.; Blakers, A.; Weber, K.; White, T. P.; Catchpole, K. R. Semitransparent Perovskite Solar Cell With Sputtered Front and Rear Electrodes for a Four-Terminal Tandem. *IEEE J. Photovoltaics* **2016**, *6*, 679–687.

(43) Fu, F.; Feurer, T.; Weiss, T. P.; Pisoni, S.; Avancini, E.; Andres, C.; Buecheler, S.; Tiwari, A. N. High-Efficiency Inverted Semi-Transparent Planar Perovskite Solar Cells in Substrate Configuration. *Nat. Energy* **2016**, *2*, 16190.

(44) Albrecht, S.; Saliba, M.; Correa Baena, J. P.; Lang, F.; Kegelmann, L.; Mews, M.; Steier, L.; Abate, A.; Rappich, J.; Korte, L.; Schlatmann, R; Nazeeruddim, M. K.; Hagfeldt, A.; Grätzel, M.; Rech, B. Monolithic Perovskite/Silicon-Heterojunction Tandem Solar Cells Processed at Low Temperature. *Energy Environ. Sci.* **2016**, *9*, 81–88.

(45) Guerrero, A.; You, J.; Aranda, C.; Kang, Y. S.; Garcia-Belmonte, G.; Zhou, H.; Bisquert, J.; Yang, Y. Interfacial Degradation of Planar Lead Halide Perovskite Solar Cells. *ACS Nano* **2016**, *10*, 218–224.

(46) Kato, Y.; Ono, L. K.; Lee, M. V.; Wang, S.; Raga, S. R.; Qi, Y. Silver Iodide Formation in Methyl Ammonium Lead Iodide Perovskite Solar Cells with Silver Top Electrodes. *Adv. Mater. Interfaces* **2015**, *2*, 2–7.

(47) Gao, L.; Zhao, E.; Yang, S.; Wang, L.; Li, Y.; Zhao, Y.; Ma, T. Light Engineering for Bifacial Transparent Perovskite Solar Cells with High Performance. *Opt. Eng.* **2017**, *56*, 1.

(48) Fu, F.; Feurer, T.; Jäger, T.; Avancini, E.; Bissig, B.; Yoon, S.; Buecheler, S.; Tiwari, A. N. Low-Temperature-Processed Efficient Semi-Transparent Planar Perovskite Solar Cells for Bifacial and Tandem Applications. *Nat. Commun.* **2015**, *6*, 1–9.

(49) Hanmandlu, C.; Chen, C. Y.; Boopathi, K. M.; Lin, H. W.; Lai, C. S.; Chu, C. W. Bifacial Perovskite Solar Cells Featuring Semitransparent Electrodes. *ACS Appl. Mater. Interfaces* **2017**, *9*, 32635–32642.

(50) Ram, O.; Bronnbauer, C.; Levchuk, I.; Hou, Y.; Brabec, C. J.; Forberich, K. Coloring Semitransparent Perovskite Solar Cells via Dielectric Mirrors. *ACS Nano* **2016**, *10*, 5104–5112.

(51) Xie, M.; Lu, H.; Zhang, L.; Wang, J.; Luo, Q.; Lin, J.; Ba, L.; Liu, H.; Shen, W.; Shi, L.; Ma, C. Q. Fully Solution-Processed Semi-Transparent Perovskite Solar Cells With Ink-Jet Printed Silver Nanowires Top Electrode. *Sol. RRL* **2018**, *2*, 1770152.

(52) Wahl, T.; Hanisch, J.; Meier, S.; Schultes, M.; Ahlswede, E. Sputtered Indium Zinc Oxide Rear Electrodes for Inverted Semitransparent Perovskite Solar Cells without Using a Protective Buffer Layer. *Org. Electron. physics, Mater. Appl.* **2018**, *54*, 48–53.

(53) Zhao, J.; Brinkmann, K. O.; Hu, T.; Pourdavoud, N.; Becker, T.; Gahlmann, T.; Heiderhoff, R.; Polywka, A.; Görrn, P.; Chen, Y.; Cheng, B; Riedl, T. Self-Encapsulating Thermostable and Air-Resilient Semitransparent Perovskite Solar Cells. *Adv. Energy Mater.* **2017**, *7,* 1602599.

(54) Chang, C. Y.; Lee, K. T.; Huang, W. K.; Siao, H. Y.; Chang, Y. C. High-Performance, Air-Stable, Low-Temperature Processed Semitransparent Perovskite Solar Cells Enabled by

Atomic Layer Deposition. *Chem. Mater.* **2015**, *27*, 5122–5130.

TABLE OF CONTENTS